Applied Catalysis B: Environment and Energy 344 (2024) 123616

Contents lists available at ScienceDirect

Applied Catalysis B: Environmental

journal homepage: www.elsevier.com/locate/apcatb

Unraveling the role of Co(II)-phosphate complex in trace Co(II) activated peroxymonosulfate process for water decontamination with phosphate surrounding

Cheng Cheng [b,c], Mopeng Xiong [a], Lin Ding [a,*], Yu Peng [a], Bo Wen [d,e], Xiao Xiao [a], Hui Zhang [c], Xiaoguang Duan [b], Wei Ren [a,b,**], Xubiao Luo [a,f]

[a] Key Laboratory of Jiangxi Province for Persistent Pollutants Control and Resources Recycle, Nanchang Hangkong University, Nanchang 330063, China
[b] School of Chemical Engineering, The University of Adelaide, Adelaide, SA 5005, Australia
[c] Department of Environmental Science and Engineering, School of Resource and Environmental Sciences, Wuhan University, Wuhan 430079, China
[d] Jiangxi Vitality Environment Technology Co. Ltd, Nanchang 330038, China
[e] Hunan GrandEco Environment Technology Co. Ltd, Changsha 410006, China
[f] School of Life Science, Jinggangshan University, Ji'an 343009, China

ARTICLE INFO

Keywords:
Peroxymonosulfate
Phosphate
Ligand effects
Electronic structure
Proton transfer

ABSTRACT

The evolution and role of Co(II)-phosphate complex in pH-dependent peroxymonosulfate (PMS) activation by trace Co(II) for phosphate-contained water decontamination was experimentally and theoretically investigated. The HPO_4^{2-} species play the most positive effect through forming Co-HPO_4 coordination for enhancing radical generation and pharmaceutical degradation (3.59 times) in neutral condition. The reduction of Co(III) to Co(II) was identified as a proton-coupled electron transfer process. In Co(II)/PMS system without phosphate, the protons from the neighboring H_2O coordination will bind with the generated $SO_4^{\bullet-}$, inducing proton poisoning effect and in situ radical quenching. While the HPO_4^{2-} coordination not only modulates the Co 3d electronic structure to optimize the PMS interaction and charge transfer, but also alters the proton affinity to alleviate the proton poisoning effect, securing the radical generation. This study provides insights into the impacts of background factors on advanced oxidation processes and develops strategies for efficient remediation in real (waste) water matrix.

1. Introduction

Advanced oxidation processes (AOPs) stand as forefront wastewater technologies, utilizing highly reactive radicals to eliminate recalcitrant organic pollutants [1]. The typical AOPs Fenton reaction (Fe(II)/H_2O_2) can generate hydroxyl radical ($^{\bullet}OH$) for pollutant abatement. An alternative reaction, Co(II)/peroxymonosulfate (PMS) system producing sulfate radical ($SO_4^{\bullet-}$), has gained substantial research interest due to the stronger oxidizing capacity (2.6−3.1 V_{NHE}) and longer lifetime (30−40 μs) of $SO_4^{\bullet-}$ than $^{\bullet}OH$ (2.8 V_{NHE} and 20 ns) [2–5]. However, these radical oxidation processes are susceptible to the interference of water matrix involving inorganic ions and natural organic matters, which limit their practical application [6,7]. Some studies found that the removal efficiency of organic pollutants in radical oxidation pathway could be promoted by the specific organic/inorganic compounds [8,9]. For example, i) several reductants can facilitate the redox cycle of metal ions for enhancing the radical generation, such as hydroquinone [10], polyphenols [11], and tetrahydroxydiboron [12]. ii) Some ligands can controllably modulate the precipitation and electronic properties of central metal to accelerate the oxidation rate of targeted pollutants, such as ethylene diamine tetraacetic acid (EDTA) [13], ethylenediamine-*N,N′*-disuccinic acid (EDDS) [14], and phosphate [15]. However, organic compounds (reductants and ligands) could be decomposed by radical attack and cause radical scavenging and potential secondary pollution, resulting in a great challenge in radical-based decontamination [16]. Therefore, the exploration of harmless inorganic compounds is a

* Corresponding author.
** Corresponding author at: Key Laboratory of Jiangxi Province for Persistent Pollutants Control and Resources Recycle, Nanchang Hangkong University, Nanchang 330063, China.
E-mail addresses: dinglin_hust@126.com (L. Ding), renwei9528@163.com (W. Ren).

https://doi.org/10.1016/j.apcatb.2023.123616
Received 5 October 2023; Received in revised form 16 November 2023; Accepted 1 December 2023
Available online 17 December 2023

promising way to ameliorate the catalytic activity of metal ions for enhancing the oxidizability and flexibility of AOPs.

Phosphate ions are widely used as pH buffer compounds in chemical analysis and synthesis, owing to three Brønsted conjugate acid-base pairs that possess proton donating or accepting capacities [17–19]. Phosphates ubiquitously distribute in surface water and are one of the most universal phosphoric components in some industrial wastewaters, with concentrations ranging from several to hundreds of mM [17,20,21]. Recently, it is reported that phosphates also exhibit decent catalytic ability for PMS activation to generate radicals [22–25]. Moreover, phosphate could reinforce the performance of Co(II)/PMS system even in a trace Co(II) concentration lower than emission limits (e.g., 17.5 μM of Chinese National Standard GB 25467–2010) [15]. However, the roles of phosphate in enhancing PMS activation in Co(II)/PMS system remain ambiguous. Some studies proposed that phosphate induces the formation of Co(II)-phosphate complex, wherein the phosphate ligand donates electrons to Co center for the acceleration of Co(III) reduction to Co(II) [15]. This process shares the similar promotion mechanism to the organic ligands. The organic ligands typically feature multiple electron-donating functional groups to coordinate with metal center into a multidentate structure, thus offering sufficient electron donation for the reduction of high-valence-state metals (Figure S1) [14,26–28]. Actually, phosphate exhibits a preference for monodentate mononuclear coordination with Co(II) to form a $CoHPO_4$ structure due to its higher stability constant value (log β of 15.5) than that with polyphosphates (log β of 7.9 for $P_2O_7^{4-}$ and 9.7 for $P_3O_{10}^{5-}$) [29,30]. However, this monodentate mononuclear coordination usually possesses weaker electron transfer capacity. Therefore, it is questionable that if phosphate ligand, albeit acting as a Lewis base, can furnish an adequate electron supply for the reduction of high-valence-state metals akin to organic ligands. Another unique nature of phosphate ligand is the proton donating and accepting ability. The transition metal-based PMS activation usually undergoes an electron transfer process [2,3]. However, recent investigations demonstrated the significant role of protons in affecting the generation of reactive oxygen species (ROS) in cobalt-based PMS activation system [31,32]. Nevertheless, the potential modulation of proton involvement by phosphate remains largely unexplored. Moreover, phosphate exists in various forms (H_3PO_4, $H_2PO_4^-$, HPO_4^{2-}, and PO_4^{3-}) depended on the solution pH. The different species forms possess different stability constants, electron-modulating capacities, and proton-donating capacities. However, their effects on the enhancement of PMS activation remains ambiguity, demanding comprehensive investigation.

In this study, we revisited the phosphate enhanced PMS activation process with trace Co(II) and evaluated the role of the Co(II)-phosphate complex in enhancing the generation of ROS for pollutant degradation. Two kinds of pharmaceutical and personal care products (PPCPs), chloroquine phosphate (CQP) and sulfamethoxazole (SMX), were selected as targeted pollutants to evaluate the activity of Co(II)+phosphate/PMS system. The dominant ROS were identified and quantified at various pHs by electron paramagnetic resonance (EPR), chemical quenching, quantitative structure-activity relationships (QSARs) and kinetic model calculation. More importantly, the proton-coupled electron transfer (PCET) process of cobalt catalysis was investigated by electrochemical analysis. The role of the most pivotal HPO_4^{2-} coordination in modulating the electronic structure of the Co center and altering the proton reaction behavior was unraveled experimentally, combined with the density functional theory (DFT) calculation. Then the mechanism of enhanced PMS activation by Co(II)-phosphate complex was proposed. This study is believed to not only shed light on the activity regulation of metal center by inorganic ligand, but also advance the development of sustainable AOPs for efficient water purification utilizing ubiquitous phosphate.

2. Experimental section

2.1. Chemical and reagents

The chemical and reagents used in this study can be seen in Text S1 in Supporting Information.

2.2. Experimental procedure

Reactions were initiated by dosing certain volumes of $CoSO_4 \bullet 7H_2O$ and PMS stock solutions into the solution containing phosphate and CQP or other chemicals, in which the pH was first adjusted to the desired value. Typically, the Co(II) and phosphate concentration were selected as 0.8 μM and 4.0 mM, which were the concentrations below the emission limits and of interests in industrial wastewaters from pharmaceutical production (3−10 mM) [21], respectively. At predetermined time intervals, 1.0 mL of aliquot sample was collected and quickly filtered through 0.22 μm polyether sulfone filters, followed by the successive addition of 10 μL of methanol (MeOH), dimethyl sulfoxide (DMSO), and acetic acid to quench the reaction for the further analysis. All experiments were conducted in duplicate or triplicate, and the mean and its standard deviations were presented.

2.3. Analytical methods

The concentration of organic pollutants and chemical probes was quantified by Waters 1525 high performance liquid chromatography (HPLC) with a UV-Vis detector and a C18 column (4.6 × 250 mm × 5 μm). The detection details were presented in Table S1. The pseudo-first-order kinetic equation was used to determine the reaction rate constant (k_{obs}) of pollutant removal. The transformation products of CQP were identified with HPLC-Q-TOF MS/MS (Xeyo G2-Q-Tof, Waters) (Text S2). The ROS were qualitatively detected on an EPR spectrometer (Bruker ESR 5000) (Text S2) and quantitatively calculated using a competition kinetic method (Text S3). The formation of Co(II)-phosphate complex was detected by Raman spectroscopy (Horiba Scientific) equipped with a green laser (532 nm). The redox potentials of Co(II) with or without the phosphate were determined by cyclic voltammetry (CV) measurements on an electrochemical workstation (CHI 760E, Shanghai Chenhua) (Text S2).

2.4. DFT calculations

The DFT calculations of the electrostatic potential, molecular orbitals (MO), and Fukui functions were carried out using the DMol3 module in the Gaussian 09 program [33]. Other DFT calculations regarding electronic structure are performed with the projector augmented plane-wave method, as implemented in the Vienna ab initio simulation package [34]. The details could be found in Text S4 in Supporting Information.

3. Results and discussion

3.1. Performance and ROS in Co(II)+phosphate/PMS system

As shown in Fig. 1a, CQP was barely degraded (< 5%) by Co(II) alone or PMS alone at pH 6.5. It was reported that phosphate possesses the capability to activate PMS generating radicals such as $^{\bullet}OH$ and $SO_4^{\bullet -}$ [20,35]. Nevertheless, only partial CQP (8.2%) was removed in the phosphate/PMS system. Conversely, CQP was obviously degraded when PMS was activated by Co(II), indicating that Co(II) exhibits superior catalytic activity for PMS activation even at a trace concentration (0.8 μM). Notably, CQP could be completely removed within 10 min after adding phosphate into Co(II)/PMS system with a pseudo-first-order reaction rate constant of 0.671 min^{-1}, which was about 3.5 times higher than that for the Co(II)/PMS system (0.172 min^{-1}) (Fig. 1b). This result

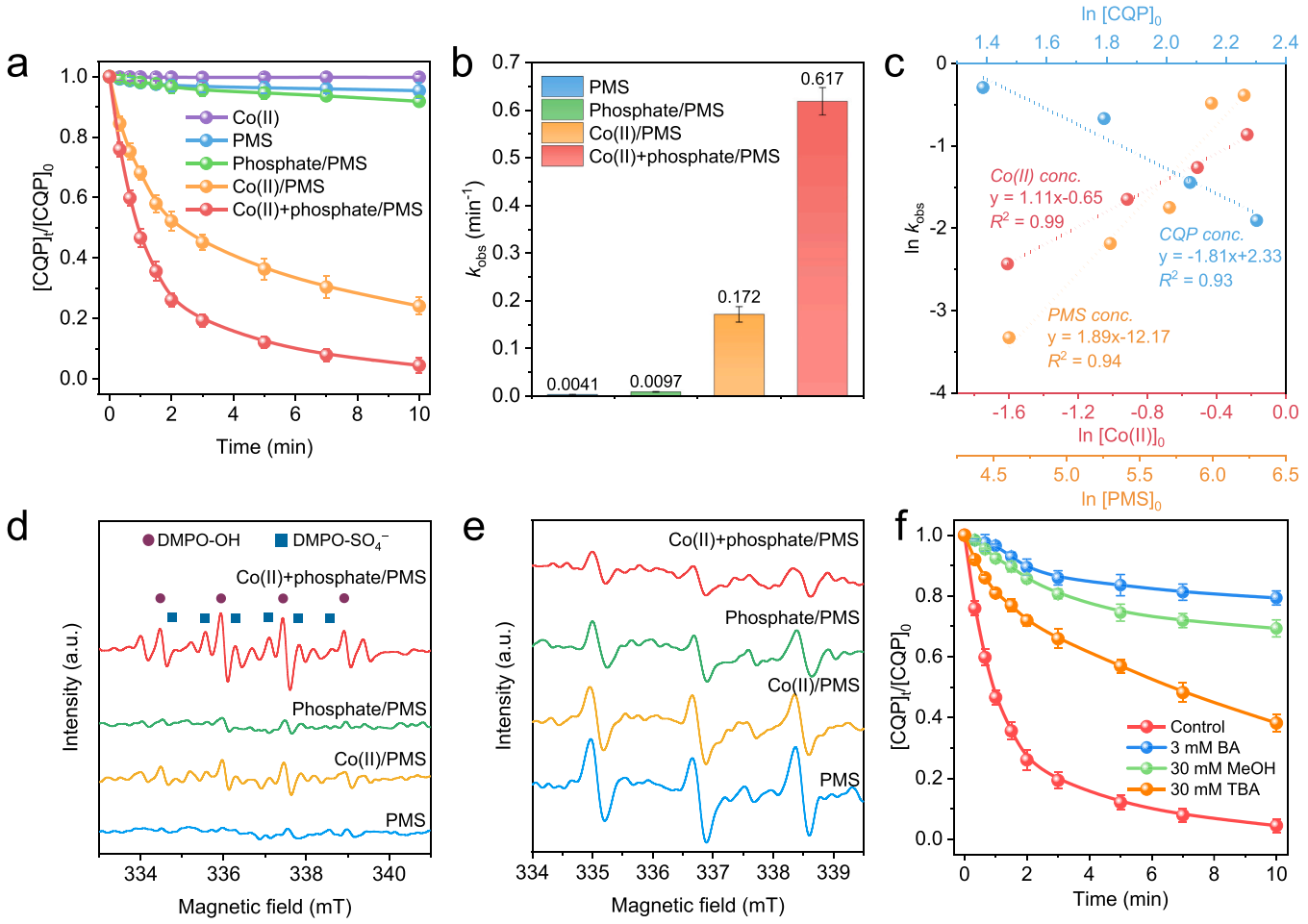

Fig. 1. (a) Degradation of CQP in different systems and (b) the corresponding reaction rate constants. (c) Correlations of reaction rate constants to Co(II) concentration, PMS concentration, and CQP concentration. EPR spectra of different systems using (d) DMPO and (e) TEMP as trapping agents. (f) Effect of different quenchers on CQP degradation in Co(II)+phosphate/PMS system. Conditions: [CQP] = 6.0 μM, [Co(II)] = 0.8 μM, [phosphate] = 4.0 mM, [PMS] = 0.4 mM, [DMPO] = 100 mM, [TEMP] = 50 mM, [MeOH] = [TBA] = 30 mM, [BA] = 3.0 mM, pH 6.5.

suggested that phosphate could enhance the reaction efficiency of Co(II)/PMS with a trace Co(II) concentration, consistent with the previous study [15]. The kinetic of Co(II)+phosphate/PMS system was also investigated at various dosages of catalyst, oxidant, and organic contaminants. As shown in Figure S2a and S2d, the oxidation rate constants for CQP exhibited gradual augmentation from 0.088 to 0.617 min^{-1} with increased Co(II) concentration from 0.2 to 0.8 μM. Similarly, an elevation of PMS concentration from 0.1 to 0.5 mM led to an increase of oxidation rate constant from 0.036 to 0.680 min^{-1} (Figure S2b and S2e). Conversely, the rise in CQP concentration led to the deceleration of its oxidation rate (Figure S2c and S2f). The corresponding correlations of ln ([Co(II)]), ln ([PMS]), and ln ([CQP]) to ln k_{obs} were established, respectively (Fig. 1c). The overall reaction rate under the present experimental conditions can be expressed in eq. 1 with a unit of μM min^{-1} (Text S5). The reaction order in PMS concentration (1.89) surpassed that in Co(II) concentration (1.11), indicating that the PMS decomposition might be the key step determining the reaction rate for the CQP removal.

$$v = \frac{dc}{dt} = 3.89 \times 10^{-5}[\mathrm{PMS}]^{1.89}[\mathrm{Co(II)}]^{1.11} \quad (1)$$

The generated ROS were first identified by EPR. As shown in Fig. 1d, when 5,5-dimethyl-1-pyrroline-*N*-oxide (DMPO) was employed as spin-trapping agent, the characteristic signals of DMPO-$SO_4^{\bullet-}$ (a_H = 1.01 mT, a_N = 1.39 mT, $a_{H\gamma}$ = 0.14 mT, and $a_{H\beta}$ = 0.06 mT) and DMPO-OH (a_H = a_N = 1.49 mT) were clearly observed in both Co(II)/PMS and Co(II)+phosphate/PMS systems, suggesting the presence of $SO_4^{\bullet-}$ and/or $^{\bullet}OH$ in these system. The intensity of signals in Co(II)+phosphate/PMS system markedly exceeded that observed in Co(II)/PMS system, indicating the enhanced generation of radicals by phosphate, consistent with the CQP degradation results in Fig. 1a. The potential generation of $^1O_2$ was then determined using 2,2,6,6-tetramethyl-4-piperidinol (TEMP) as spin-trapping agent. A characteristic three-line signal corresponding to 2,2,6,6-tetramethylpiperidine-*N*-oxyl (TEMPO; a_N = 1.71 mT) was observed when PMS was solely added (Fig. 1e). This signal, indicative of the potential generation of $^1O_2$, might stem from the self-decomposition of PMS under neutral pH conditions or the direct PMS oxidation [36,37]. However, the intensity of signals was attenuated with the introduction of both Co(II) and phosphate, suggesting a limited contribution of $^1O_2$ to pollutant removal in Co(II)+phosphate/PMS system. Recent studies have reported the generation of high-valent cobalt-oxo species (Co(IV)) that dominated the pollutant degradation in the Co(II)/PMS system [7,31]. Co(IV) could be detected using methyl phenyl sulfoxide (PMSO) as chemical probe, which can be selectively oxidized to methyl phenyl sulfone ($PMSO_2$) by Co(IV) via oxygen atom transfer pathway [18]. However, the oxidation of PMSO and the generation of $PMSO_2$ in Co(II)+phosphate/PMS system were almost identical to those in the phosphate/PMS system (Figure S3). Thus, the generation of Co(IV) in the present system was ruled out. This is primarily due to the strong dependence of Co(IV) generation on the Co(II)/PMS ratio and pH, such as Co(II)/PMS ratios exceeding 1:10 in an acid environment, which are unfit for the present system, i.e., a lower Co(II)/PMS molar ratio (1:500)

at neutral pH [7,31]. Furthermore, the potential contribution of direct Co(III) oxidation was also ruled out, given the extremely low concentration of free Co(III) in water solution (approximately 1.6×10^{-23} M at pH 6.5) when introducing 0.8 μM Co(III) into water [38]. Therefore, the major ROS generated in Co(II)+phosphate/PMS system were identified as $SO_4^{\bullet-}$ and/or $^{\bullet}OH$.

The contribution of $SO_4^{\bullet-}$ and/or $^{\bullet}OH$ to CQP degradation was further elucidated by chemical quenching experiments, where *tert*-butanol (TBA) was used as a quencher of $^{\bullet}OH$, while MeOH and benzoic acid (BA) were used as quenchers of both $SO_4^{\bullet-}$ and $^{\bullet}OH$ [39–41]. As shown in Fig. 1f and Figure S4, the CQP degradation rate was decreased from 0.617 to 0.182, 0.079, and 0.048 min^{-1} after the addition of TBA, MeOH, and BA, respectively. This result indicates that $SO_4^{\bullet-}$ and $^{\bullet}OH$ were the dominant ROS for CQP degradation in Co(II)+phosphate/PMS system. Moreover, the steady-state concentrations of $SO_4^{\bullet-}$ ($[SO_4^{\bullet-}]_{ss}$) and $^{\bullet}OH$ ($[^{\bullet}OH]_{ss}$) were determined as 2.61×10^{-13} and 2.87×10^{-13} M, respectively (Figure S5 and Table S3), using competition kinetic method using BA and nitrobenzene (NB) as probes. Then the theoretical contribution of $SO_4^{\bullet-}$ and $^{\bullet}OH$ to CQP degradation can be determined as 47.1% and 32.9%. Although $[^{\bullet}OH]_{ss}$ was marginally higher than $[SO_4^{\bullet-}]_{ss}$, the higher second-order reaction rate constant between CQP and $SO_4^{\bullet-}$ ($k_{SO_4^{\bullet-},CQP} = 1.4 \times 10^{10}$ M^{-1} s^{-1}) than that with $^{\bullet}OH$ ($k_{^{\bullet}OH,CQP} = 8.9 \times 10^{9}$ M^{-1} s^{-1}) delivered higher oxidation contribution from $SO_4^{\bullet-}$. The contributions of other species (expect $SO_4^{\bullet-}$ and $^{\bullet}OH$) were about 20%. This outcome aligns well with the chemical quenching results (blue line in Fig. 1f), indicating the reliability of the calculated $[SO_4^{\bullet-}]_{ss}$ and $[^{\bullet}OH]_{ss}$. The other species might stem from PMS direct oxidation enhanced by phosphate or the formation of the Co (II)-PMS complex [6].

The degradation pathways of CQP were further proposed based on the identified oxidation products and DFT calculations. The orbital and electronic properties of CQP were calculated, including the highest occupied molecular orbital (HOMO), electrostatic potential (ESP), and the Fukui index related to electrophilic attack (f^-). The results indicate the N atoms on the side chain of CQP are susceptible to radical attack (Fig. 2) [42]. Four major pathways for CQP degradation were proposed, involving dealkylation, deamination, ethylation and dechlorination processes (Figures S6–S14). Finally, CQP was progressively transformed into ring-opened and lower molecular weight organic products, and then mineralized into H_2O, CO_2, and inorganic ions. Comprehensive details are provided in Text S6.

3.2. Role of phosphate and pH dependence

Considering the direct relationship between the species form of phosphate and solution pH, the role of phosphate was assessed at various reaction pHs. In the phosphate/PMS system, the degradation efficiency of CQP gradually increased as pH was elevated from 3.0 to 9.5. However, further elevating the pH to 11.0 resulted in a decline in CQP degradation efficiency (Figure S15a). The Co(II)/PMS system also showed a similar trend with an optimal pH of 6.5 yielding a CQP degradation efficiency of 76% (Figure S15b). In Co(II)+phosphate/PMS system, the pH dependence of CQP degradation was quite identical to that in Co(II)/PMS system, albeit with a much enhanced degradation efficiency under all pH conditions (Fig. 3a). This trend became particularly evident when comparing k_{obs} for CQP degradation (Fig. 3b). To

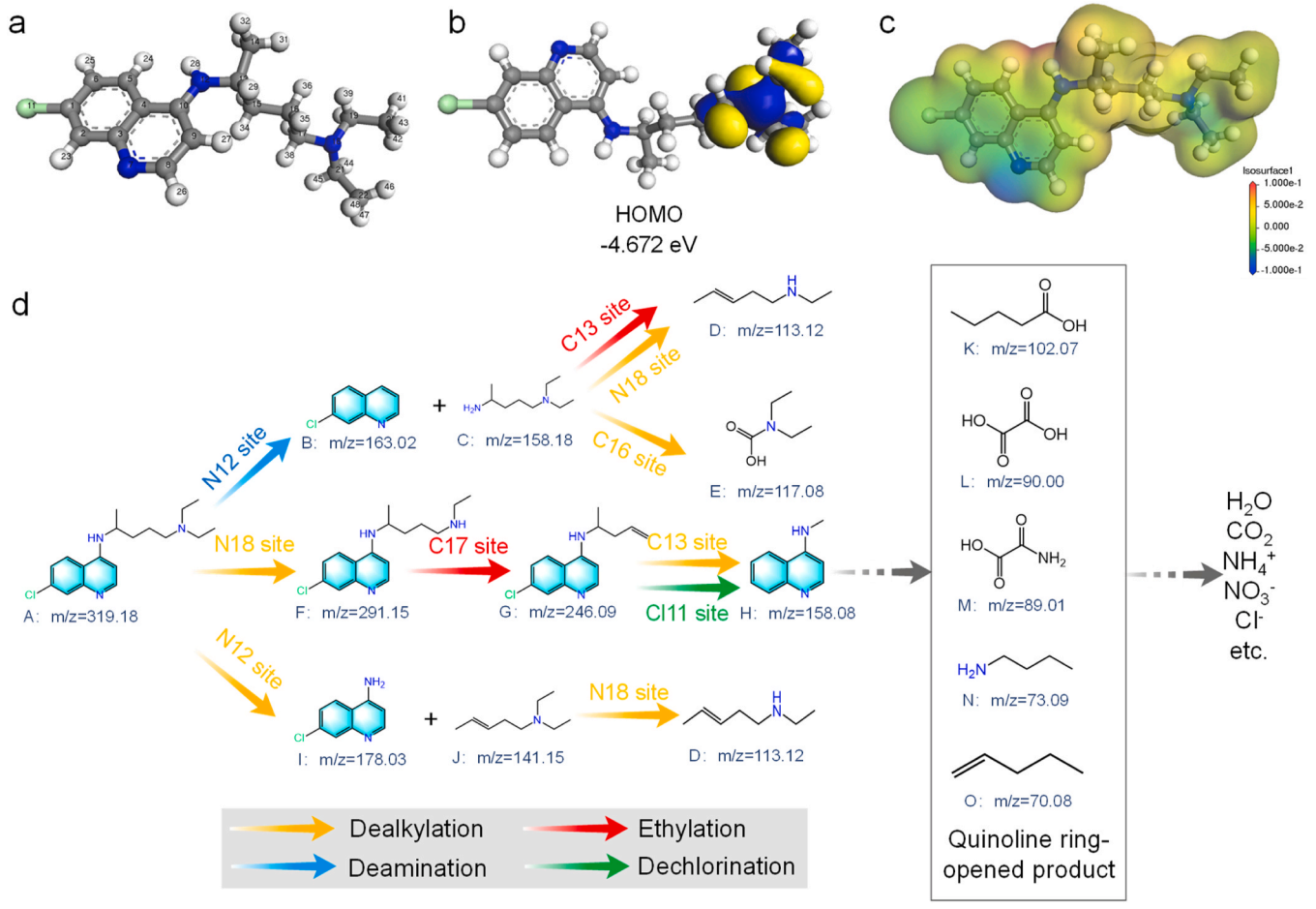

Fig. 2. (a) Chemical structure, (b) HOMO orbital, and (c) electrostatic potential distribution of CQP. (d) Proposed degradation pathway of CQP in Co(II)+phosphate/PMS system.

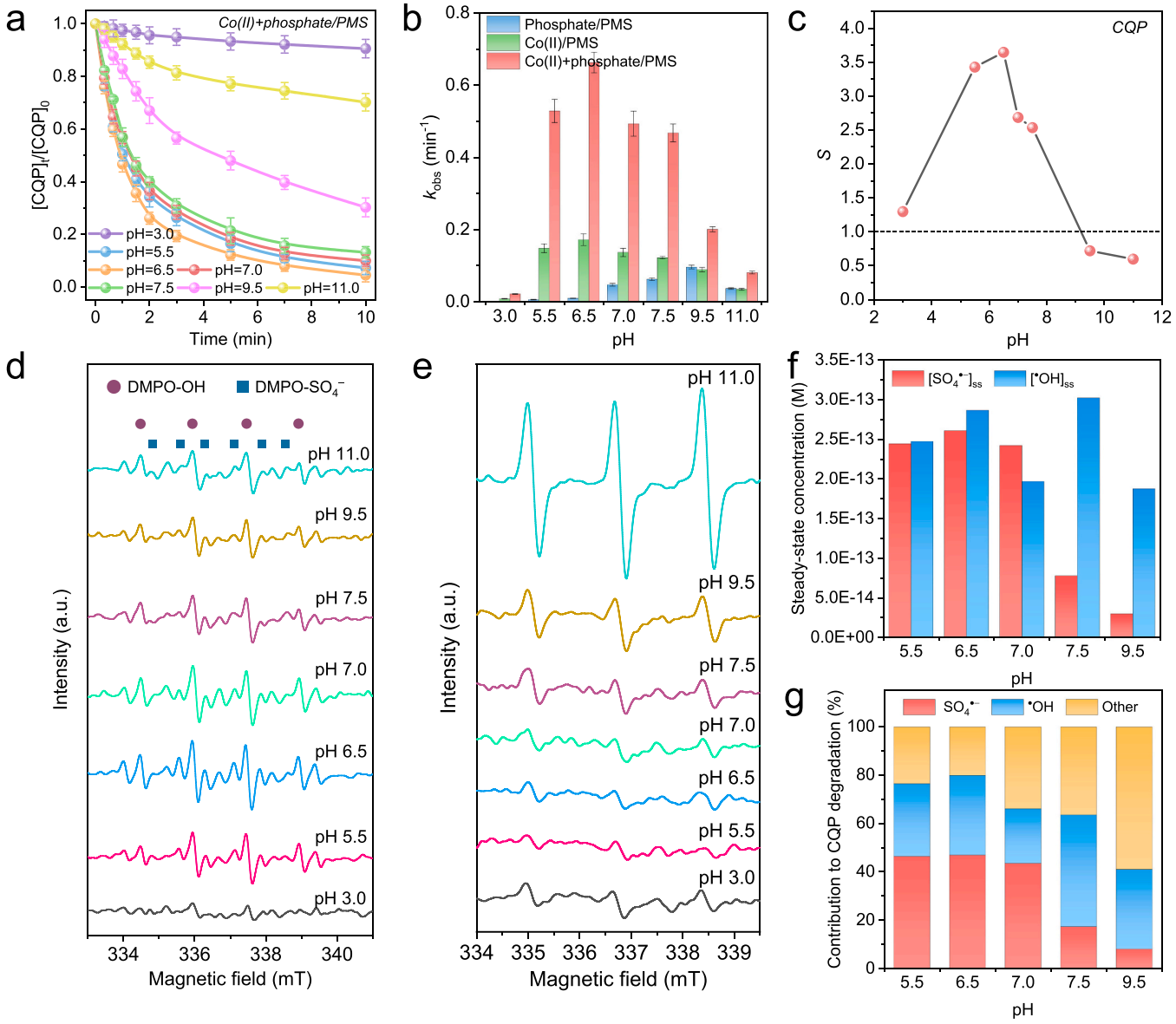

Fig. 3. (a) Effect of pH on CQP degradation in Co(II)+phosphate/PMS system. (b) Effect of pH on CQP degradation rate constants in different systems. (c) Synergistic index of Co(II) and phosphate for PMS activation for CQP degradation at different pHs. Effect of pH on EPR signals using (d) DMPO and (e) TEMP as trapping agents. Calculated (f) $[^{\bullet}OH]_{ss}$ and $[SO_4^{\bullet-}]_{ss}$ and (g) their contribution to CQP degradation in Co(II)+phosphate/PMS system at different pH. Conditions: [CQP] = 6.0 μM, [Co(II)] = 0.8 μM, [phosphate] = 4.0 mM, [PMS] = 0.4 mM, [DMPO] = 100 mM, [TEMP] = 50 mM.

further investigate the interaction between Co(II) and phosphate in PMS activation, the synergistic index (S) was calculated via eq. 2 [43]. It is noted that the values of $S > 1.0$ were observed at pH values ranging from 3.0 to 7.5, indicating the obvious synergistic effect between Co(II) and phosphate on PMS activation (Fig. 3c). The highest S values (3.6) occurred at pH 6.5 for the degradations of CQP (Fig. 3c). The similar result was also observed in the degradation of other pollutants, such as SMX (Figure S16). Therefore, the enhanced pollutant degradation efficiency was attributed to the strongest synergistic interplay between Co(II) and phosphate in PMS activation.

$$S = \frac{k_{obs}[\mathrm{Co(II)} + \mathrm{Phosphate/PMS}]}{k_{obs}[\mathrm{Co(II)/PMS}] + k_{obs}[\mathrm{Phosphate/PMS}]} \quad (2)$$

The effect of pH on ROS generation was further evaluated. EPR results show a substantial enhancement in the intensity of DMPO-SO_4^{-} and DMPO-OH signals within the pH ranges of 5.5 to 11.0 in the Co(II)+phosphate/PMS system, and the intensity of EPR signal reached maximum at pH 6.5 (Fig. 3d and Figure S17). This trend was consistent with the degradation patterns of CQP and SMX. Interestingly, it was observed that the intensity of TEMPO became greater with the increase of pH (Fig. 3e). However, the activation of Co(II) and phosphate did not elevate $^1O_2$ generation compared to PMS alone within the pH range of 3.0 to 7.5 (Figure S18), but an intensified TEMPO signal was discernible at pH 9.5 and 11.0, due to the enhanced PMS activation by phosphate under alkaline condition [23]. The $[SO_4^{\bullet-}]_{ss}$ and $[^{\bullet}OH]_{ss}$ in Co(II)+phosphate/PMS system at different pH were further calculated (Fig. 3f and Table S3). The $[SO_4^{\bullet-}]_{ss}$ hovered around $2.4–2.6 \times 10^{-13}$ M within the pH range of 5.5 to 7.0, peaking at pH 6.5 (2.61×10^{-13} M) and significantly dropping to 3.02×10^{-14} M when pH further elevated to 9.5. The $[^{\bullet}OH]_{ss}$ manifested concentrations of approximately $2.0–2.8 \times 10^{-13}$ M within the pH range of 5.5 to 7.0. The highest total concentration of radicals (sum of $[SO_4^{\bullet-}]_{ss}$ and $[^{\bullet}OH]_{ss}$) was manifest at pH 6.5, while the lowest concentration was evident at pH 9.5, which were also consistent with the degradation trends of organics. Finally, the effect of pH on the contribution of different ROS to CQP degradation was evaluated. As shown in Fig. 3g, the CQP degradation in Co(II)+

phosphate/PMS primarily relies on radicals in weak acid or neutral environment, but nonradical oxidation became dominant in weak alkaline solutions (increased from 20.0% to 58.8% with pH increased from 6.5 to 9.5).

The species distribution of Co(II), phosphate, PMS, and pollutants all varied with changing pH. The pollutants in their ionic states often exhibit higher reactivity but concurrently confront augmented electrostatic repulsion from negatively charged reactive species such as $SO_4^{\bullet-}$ [44]. The shared optimal pH and maximum synergistic effects among pollutants with different pK_a values (pK_a of 8.1 for CQP and 5.6 for SMX) in the Co(II)+phosphate/PMS system implied that the effect of pollutant molecular/ionic state on degradation was negligible, due to the nonselective radical oxidation. Similarly, the role of PMS activation by phosphate appeared insignificant, and further discussion was presented in Text S7. Therefore, the enhanced PMS activation activity might be governed by the Co(II) species variation at different pH and the presence of phosphate. Specifically, the optimal CQP degradation efficiency in the Co(II)/PMS system was obtained under neutral pH conditions, suggesting that $Co(OH)^+$ constituted the most active species for PMS activation (Figure S19) [45]. However, the presence of phosphate could trigger the formation of Co(II)-phosphate complex, such as $CoHPO_4$, which has been reported to possess pronounced reactivity in PMS activation (Figure S19) [15]. To quantitatively evaluate the impact of Co(II)-phosphate complex on PMS activation, a multiple linear regression analysis was performed, leveraging CQP oxidation rate constants and phosphate species concentrations across various pH values (Table S5). The resulting eq. 3 distinctly highlighted the positive influence of Co(II)-phosphate species on CQP degradation, validating the pivotal role of Co(II)-phosphate complex.

$$\ln k_{obs} = -32.43x_1 - 24.93x_2 - 25.52x_3 - 25.04x_4 + 2.78x_5 + 98.81 \quad (3)$$
$$R^2 = 0.997$$

where k_{obs} is the pseudo-first order kinetic rate constant, x_1, x_2, x_3, x_4, and x_5 are the species concentration of H_3PO_4, $H_2PO_4^-$, HPO_4^{2-}, PO_4^{3-}, and Co(II)-phosphate, respectively.

The formation of Co(II)-phosphate complex was confirmed by Raman spectroscopy. As shown in Fig. 4a, a broad peak, centered around 1500−1800 cm^{-1}, indicative of Co(II) species was observed under all the conditions [46]. Upon phosphate addition, a new peak emerged at approximately 804 cm^{-1} at pH 6.5, corresponding to ν[P−(OH)] [47]. This new peak was notably absent at pH 3.0 and 11.0, consistent with the results of the most significant synergistic effect between Co(II) and phosphate for PMS activation at pH 6.5. Furthermore, the peak attributed to Co(II) species was blue-shifted from 1560 to 1832 and 1583 cm^{-1} with increasing pH from 3.0 to 6.5 and 11.0, suggesting increased charge density of Co(II) species at pH 6.5 [48]. Hence, the formation of Co(II)-phosphate complex was identified as responsible for the enhanced PMS activation. The formation of metal-complex could modify redox potentials via ligand field effect to impact the catalytic activity of metal sites [26]. Therefore, the effect of phosphate on Co(II) redox potential at different pHs was evaluated via electrochemical analysis (Fig. 4b−d and Figure S20). For Co(II) alone, an evident oxidation peak emerged at pH 3.0, attributed to the oxidation of Co(II) to Co(III). However, the peak current weakened with pH elevation and the presence of phosphate. Electrooxidation of Co(II) ensued through outer-sphere electron transfer from solvated Co(II) to the anode [49]. At higher pH or in the presence of phosphate, formation of Co(II)

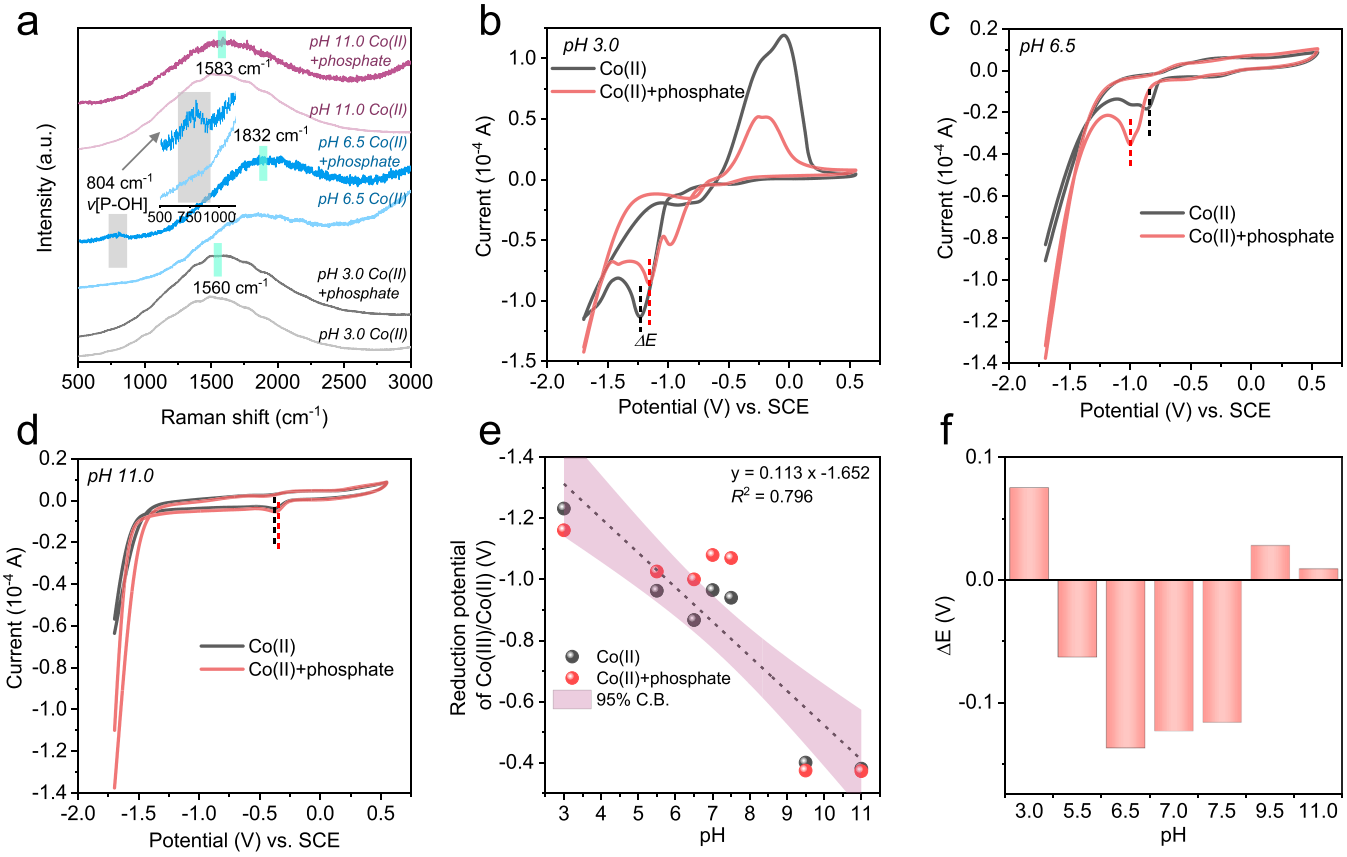

Fig. 4. (a) Raman spectra of Co(II) in the absence and presence of phosphate at different pH. CV curves in Co(II) and Co(II)+phosphate electrolytes at pH (b) 3.0, (c) 6.5, and (d) 11.0. (e) Pourbaix diagram of Co(III) reduction with or without the phosphate. (f) The differences of Co(II) reduction potential with the addition of phosphate. Conditions: [Co(II)] = 2.0 mM, [phosphate] = 4.0 mM, scan rate = 50 mV s^{-1}.

oxyhydroxide or Co(II)-phosphate complex, achieved by displacing H_2O coordination, hindered the outer-sphere electron transfer process, ultimately leading to reduced Co(II) oxidation current. Conversely, the reduction peak of Co(III) to Co(II) appeared across all pH values and demonstrated variation in peak position in both Co(II) and Co(II)+phosphate electrolytes. A linear relationship was established between the reduction potential of Co(III)/Co(II) and pH, yielding an *E*/pH slope of 0.113 V/pH (Fig. 4e). This result indicates that the reduction of Co (III) to Co(II) (with or without the phosphate) is a proton-coupled electron transfer (PCET) process, necessitating two protons for Co(III) reduction as per the Nernst equation (Text S8) [49]. In contrast, the oxidation of Co(II) to Co(III) is a direct electron transfer process without the participation of proton (Figure S21). Therefore, Co(II) oxidation and Co(III) reduction processes can be expressed as eqs. 4−9 (in neutral pH and assuming the phosphate species as HPO_4^{2-}).

$$Co^{2+} + H_2O \rightarrow CoOH^+ + H^+ \quad (4)$$

$$CoOH^+ - e^- \rightarrow CoO^+ + H^+ \quad (5)$$

$$CoO^+ + 2H^+ + e^- \rightarrow Co^{2+} + H_2O \quad (6)$$

$$Co^{2+} + HPO_4^{2-} \rightarrow CoHPO_4 \quad (7)$$

$$CoHPO_4 - e^- \rightarrow CoHPO_4^+ \quad (8)$$

$$CoHPO_4^+ + 2H^+ + e^- \rightarrow CoH_3PO_4^{2+} \quad (9)$$

The similar pH-dependent behavior of Co(III) reduction to Co(II), regardless of the presence of phosphate, suggests that the thermodynamics of the Co(III) reduction to Co(II) remain unaffected by the formation of phosphate complex (Figure S21). However, the specific redox potential values of Co(III)/Co(II) are evidently affected by the phosphate coordination. For example, the reduction potential of Co(III)/Co(II) exhibited a noticeable increase at pH 3.0 but experienced a decrease within the pH range of 5.5 to 7.5 in the presence of phosphate. While the potential variation induced by phosphate gradually diminished as pH further increases to 9.5 and 11.0 (Fig. 4f). This suggested that the addition of phosphate retarded the reduction of Co(III) to Co(II) within the pH range of 5.5 to 7.5. Interestingly, phosphate induced promotion of PMS activation primarily occurs on these pH ranges, which suggested that the Co(III)/Co(II) cycle process is not the rate-limiting step for PMS activation in Co(II)+phosphate/PMS system. $H_2PO_4^-$ and HPO_4^{2-} are dominant forms in pH ranges of 5.5 to 7.5. Both phosphates possess coordinatively unsaturated O atoms capable of attracting protons and prohibit the proton affinity to Co center, leading to the inhibition of Co (III) to Co(II) reduction by phosphate with the pH range of 5.5 to 7.5. In contrast, H_3PO_4 is the predominant species form of phosphate at pH 3.0, which exhibits a proton-donating capacity, thereby expediting the Co (III) reduction via PCET process. The change of Co(III) reduction potential between with and without phosphate was relatively negligible at pH 9.5 and 11.0, due to the gradual precipitation of Co(II)-phosphate complex to $Co_3(PO_4)_2$ under such conditions (Figure S22). Therefore, protons play pivotal role in governing the redox behavior of both Co(II) and Co(II)-phosphate complex, exerting a direct influence on PMS activation activity. Moreover, it was also reported that protons directly partake in the PMS activation process, thereby regulating selectivity of generated reactive species [32]. To comprehensively assess the impact of phosphate coordination and the intricate proton-involved reaction mechanisms for PMS activation, DFT calculations were performed to provide insights at molecular-level.

3.3. Mechanistic insights from DFT analysis

Molecular orbitals of various phosphate species, Co(II)-phosphate complex, and PMS were calculated to determine the effect of phosphate species on the electronic structure of Co(II). Specifically, the HOMO of Co(II)-phosphate complex and the lowest unoccupied molecular orbital (LUMO) of PMS were calculated. As shown in Fig. 5a, models of the Co(II)-phosphate complex were constructed based on a mononuclear monodentate configuration, considering its highest value of stability constant [29,30]. The HOMO of Co(II)-phosphate complex is mainly located at Co center. The electron-rich region, represented by the blue region, is noticeably affected by the forms of phosphate coordination [50]. The HOMO energy of Co(II)-phosphate complex increased progressively within the gradual deprotonation of phosphate, indicating an increased electron-donating capacity (Table S7). Similarly, the LUMO energy of PMS increased as its state transformed from HSO_5^- to SO_5^{2-}, suggesting a reduced electron-withdrawing ability of PMS at higher pH values (i.e., pH >9.4). The PMS activation necessitates electron transfer from the metal center for the cleavage of O−O bond. Therefore, the energy gap between LUMO of PMS and HOMO of activators can determine the PMS activation reactivity. The narrowest energy gap indicates the most facile electron transfer from activator to PMS and the fast pollutant degradation rate, which is attained between $[Co]^{2+}HPO_4^{2-}$ and HSO_5^- (3.065 eV) (Figure S23). The above results suggest that PMS activation by $[Co]^{2+}HPO_4^{2-}$ is more thermodynamically favorable. Considering that the reaction kinetic, i.e., charge transfer rate hinges on the intrinsic electronic structure of the active sites, the effect of HPO_4^{2-} coordination on the electronic structure of Co center was specifically evaluated.

Structural models for $[Co(H_2O)_6]^{2+}$ and $[Co(H_2O)_5]^{2+}HPO_4^{2-}$ are illustrated in Figure S25 and abbreviated to Co and Co-HPO_4, respectively. As displayed in Fig. 5b, electrons are transferred from Co and H atoms and then uniformly accumulate on the O atoms within the six H_2O coordination. When a HPO_4^{2-} anion coordinates with Co^{2+}, the symmetric electron distribution is disrupted, leading to the accumulation of electrons at the O atom coordinated with both Co and P atoms (Fig. 5c). Bader analysis revealed a reduction of 0.03 e in the charge of Co atoms. Then density of states (DOS) analysis for Co and Co-HPO_4 was performed. As shown in Fig. 5e, the presence of HPO_4^{2-} coordination facilitates electron delocalization in the O 2p orbital and an upshift of the Co 3d orbital to the Fermi level. Therefore, a pronounced electron occupation near the Fermi level is observed for Co-HPO_4, indicative of the enhanced reactivity. This change in DOS originates from the disruption of symmetry in the $[Co(H_2O)_6]^{2+}$ structure through HPO_4^{2-} coordination, causing the redistribution of electrons within O 2p and Co 3d orbitals. Further analysis of projected DOS (PDOS) demonstrates that the sate near the Fermi level is associated with d_{xz} and d_{x2-y2} electrons of Co atom (Fig. 5d and Figure S26) as well as the O 2p electrons of the axial H_2O coordination and the terminal O in HPO_4^{2-} (Figure S27). These results suggest that the formation of the HPO_4^{2-} complex significantly modulates the electronic structure and catalytic properties of Co(II). Then PMS adsorption behaviors are studied and the corresponding structures are denoted as Co-PMS* and Co-HPO_4-PMS* (Figure S25). While the PMS adsorption energy (E_{ads}) on Co-HPO_4 (−1.961 eV) is more negative than that on Co (−1.683 eV), the charge transfer from Co atom to the coordinated hydroxy O of PMS decreases by 0.202 e (Figs. 5f and 5g). This diminished charge transfer from Co atom originates from the charge compensation by the coordinated O of HPO_4, as supported by the accumulation of extra electrons around the Co center in Co-HOP_4 (Fig. 5g). These findings suggest that HPO_4^{2-} coordination enhances PMS adsorption and decreases the electron consumption of Co atom during the charge transfer to PMS. The DOS analysis also shows that Co-HPO_4-PMS* exhibits stronger electron delocalization and orbital overlap near the Fermi level than Co-PMS*, indicating a stronger interaction between PMS and Co through HPO_4^{2-} coordination (Fig. 5h). This reinforced interaction is related to the d_{x2-y2} electrons of Co atom (Figure S26) and O 2p electrons of the terminal O in PMS and HPO_4^{2-} (Figure S27). In addition, the PDOS of the Co 3d orbital shifts toward the negative direction with a lower d-band center (−3.309 eV) upon PMS adsorption onto the Co model. However, the PDOS shifts toward the positive direction with a higher d-band center (−1.655 eV) after PMS adsorption

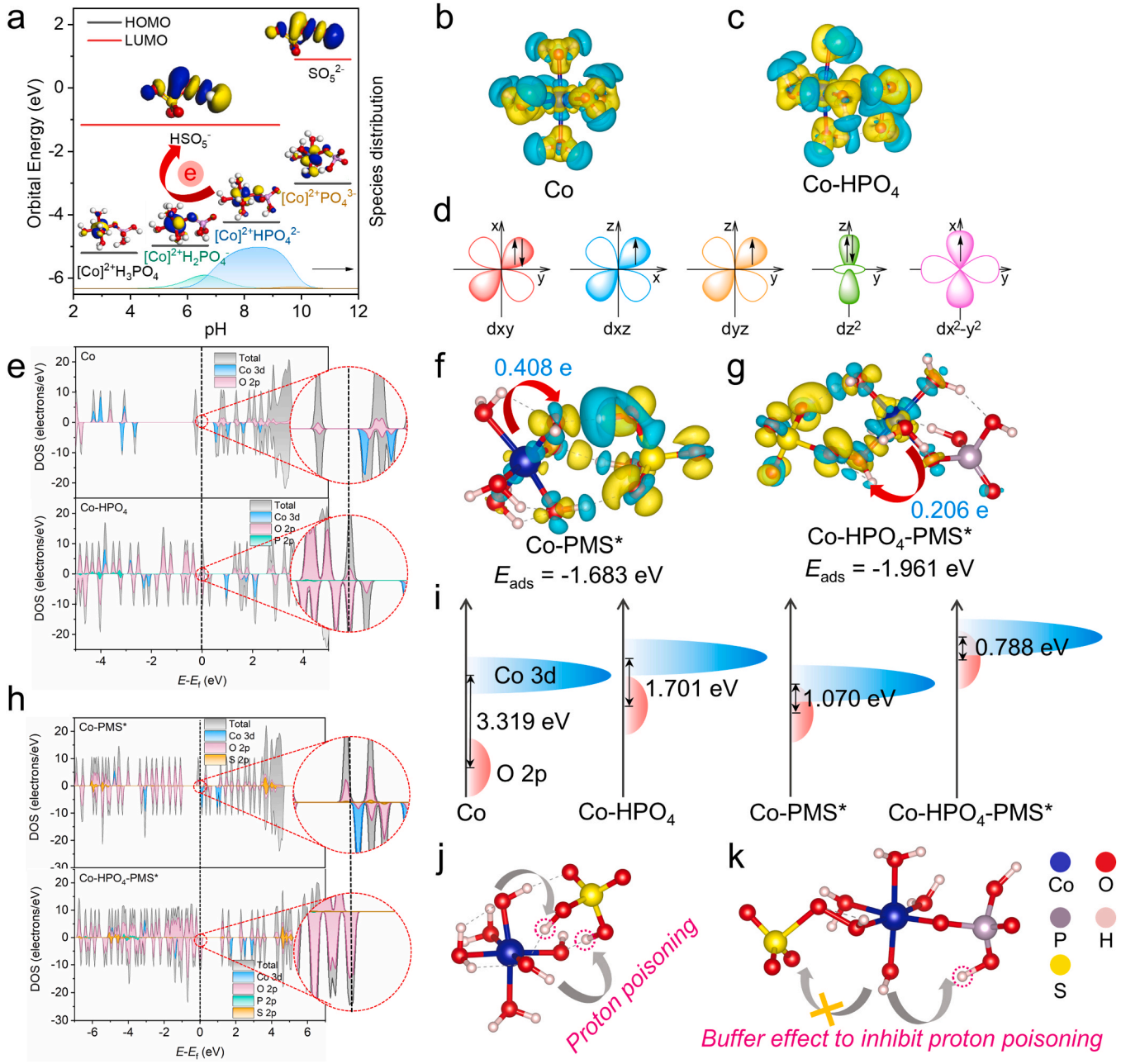

Fig. 5. (a) The LUMO level of PMS and HOMO level of Co(II)-phosphate complex in different species form. Charge density difference (CDD) for (b) Co and (c) Co-HPO_4. Yellow and cyan contours represent electron accumulation and depletion with an isosurface level of 0.007 e $Bohr^{-3}$. (d) Electron occupations of Co 3d orbital of Co-HPO_4. (e) Computed DOS in Co and Co-HPO_4. CDD for (f) Co-PMS* and (g) Co-HPO_4-PMS* with an isosurface level of 0.004 e $Bohr^{-3}$ and the corresponding charge transfer numbers and adsorption energies. (h) Computed DOS in Co-PMS* and Co-HPO_4-PMS*. (i) Schematic representation of the Co 3d- and O 2p-band for different structures and their corresponding energy overlap. (j) The proton poisoning to the generated $SO_4^{\bullet-}$ for Co-PMS*. (k) The effect of phosphate complex to inhibit proton poisoning for Co-HPO_4-PMS*.

for the Co-HPO_4 model. This suggests that HPO_4^{2-} coordination significantly modified the PMS activation process (Figure S28). The O 2p-band centers of different models are also calculated (Table S8). Fig. 5i shows that PMS adsorption enhances the overlap between Co centers and O atoms for both Co and Co-HPO_4. Notably, Co-HPO_4-PMS* possesses a substantially higher degree of overlapping, further suggesting the intensified interaction between PMS and Co through HPO_4 coordination. It is noted that in Co-PMS*, a larger charge transfer from Co to the coordinated hydroxy O atom in PMS leads to the cleavage of O—O bond and the generation of $SO_4^{\bullet-}$ [51]. However, it is observed that the protons from the neighboring H_2O coordination can promptly bind with $SO_4^{\bullet-}$ to form hydrogen bonds, resulting in in situ quenching of $SO_4^{\bullet-}$ via the proton poisoning effect (Fig. 5j). Intriguingly, in Co-HPO_4-PMS*, a modest charge transfer from the Co center to PMS initially elongates the O—O bond in PMS instead of directly cleaving it. Then a proton from the H_2O coordination is captured by HPO_4 due to its proton-accepting capacity, thus inhibiting proton poisoning (Fig. 5k). This can be considered a buffering effect at the molecule-environment (Table S9). Subsequently, the O—O bond is cleaved, resulting in the generation of more reactive $SO_4^{\bullet-}$ for Co-HPO_4. Therefore, the roles of HPO_4^{2-} coordination with Co(II) for PMS activation encompass (i) enhancing the interaction between the Co center and PMS while optimizing charge transfer by regulating the electronic structure of Co atom and (ii) constructing a local neutral environment to suppress the proton poisoning of the

radicals due to its higher proton affinity. These theoretical analyses are corroborated by the notably low PMS activation performance at pH 3.0, where the phosphate complex is mostly protonated and incapable of accepting additional protons.

3.4. Proposed enhancement mechanism by Co(II)-phosphate complex

Based on the above results, a possible mechanism is proposed for the enhanced PMS activation by the Co(II)-phosphate complex (Fig. 6). The enhanced PMS catalysis originates from the formation of Co(II)-phosphate complex, notably $[Co(H_2O)_5]^{2+}HPO_4^{2-}$ under neutral conditions, which affects the redox properties of Co(II) and PMS activation behavior. The ligand effect from HPO_4^{2-} modulates the electronic structure of Co atom to increase electron occupation at the Fermi level and upshift its 3d-band center, resulting in the enhanced PMS adsorption (increased E_{ads}) and interaction (more electron overlapping between Co 3d and O 2p orbitals). Then, HPO_4^{2-} coordination influences the number of transferred charge and behavior of proton affinity, thereby altering the destination of the generated ROS. In scenarios where PMS is activated with $[Co(H_2O)_6]^{2+}$, a greater charge transfer from Co center to PMS can directly generate $SO_4^{\bullet-}$, which tends to be quenched by protons from H_2O molecules and transformed to the inactive SO_4^{2-}. However, with HPO_4^{2-} coordination, the $[Co(H_2O)_4]^{2+}HPO_4^{2-}$-PMS interaction and moderate charge transfer first elongate the O—O bond in PMS, and proton from H_2O can be trapped by the coordinatively unsaturated O atom of phosphate complex due to ligand's proton-accepting ability. This process can prevent proton poisoning effect, consequently securing radical generation.

3.5. Practical application potential

In addition to CQP and SMX, other typical pharmaceutical drugs such as acetaminophen, ibuprofen, and carbamazepine could also undergo efficient degradation in Co(II)+phosphate/PMS system due to the enhanced generation of radicals (Fig. 7a). Then the effects of typical inorganic anions, including Cl^-, NO_3^-, SO_4^{2-}, HCO_3^-, and $HSiO_3^-$, as well as natural organic matters (NOM) on CQP degradation were investigated (Figure S29). The addition of HCO_3^- and $HSiO_3^-$ inhibited CQP degradation, which was attributed to the radical quenching effect from HCO_3^- and the coordination effect from $HSiO_3^-$, which might behave as ligand to coordinate with Co(II) and restrain the formation of Co(II)-phosphate complex (detailed in Text S9) [25,52,53]. Moreover, the CQP degradation efficiency could be maintained to some extent in various real water samples (Fig. 7b). In addition, the residual phosphate could be effectively removed by employing polyferric sulfate and $CaCl_2$ coagulation. At the optimal coagulation condition, the phosphate residual was reduced to 0.33 mg L^{-1}, which was below the surface water limit (0.4 mg L^{-1}) (Figs. 7c and 7d). Therefore, the environmental impact of phosphate could be mitigated. Considering that the concentration of Co (II) (0.8 μM) used in our study is below the permissible limits for both wastewater (17.5 μM of Chinese National Standard GB 25467–2010) and reclaimed water (0.9 μM of US Environmental Protection Agency) and the required phosphate can be directly harnessed from the industrial wastewaters from pharmaceutical production, the Co(II)+phosphate/PMS system exhibits significant potential as a sustainable, green and efficient environmental remediation technique.

4. Conclusion

Phosphate ubiquitously distribute in (waste)waters and are widely used as pH buffer compounds in chemical analysis and synthesis. Here, we revisited the phosphate enhanced PMS activation with trace Co(II) (0.8 μM) for water decontamination. The introduction of phosphate (4.0 mM) remarkably enhances the radical generation and pollutant degradation by 3.59 times. Therefore, this process holds significant promise as a technology for the treatment of industrial wastewaters from pharmaceutical production those rich in phosphate concentration during the synthesis process. The enhancement by phosphate is pH-dependent and the HPO_4^{2-} species play the most positive effect through forming Co-HPO_4 coordination under neutral conditions. The HPO_4^{2-} coordination modulates the electronic structure of Co atom by increasing the electron occupation at Fermi level, thus strengthening its interaction with PMS and optimizing the charge transfer. Then the phosphate coordination can construct a local neutral environment to suppress the proton poisoning of the radicals due to its higher proton affinity, thus securing radical generation. This study not only advances our understanding of the ligand effect in metal-based AOPs for efficient remediation in real (waste)water matrix, but also stimulates further exploration and advancement in the realm of inorganic ligands for water decontamination, especially those widely prevalent in the environment.

CRediT authorship contribution statement

Cheng Cheng: Conceptualization, Methodology, Investigation, Writing – original draft. **Mopeng Xiong:** Conceptualization, Methodology, Investigation. **Lin Ding:** Resources, Writing – review & editing, Supervision. **Yu Peng:** Methodology, Investigation. **Bo Wen:** Formal analysis, Visualization. **Xiao Xiao:** Validation, Software, Writing – review & editing. **Hui Zhang:** Writing – review & editing. **Xiaoguang Duan:** Conceptualization, Writing – review & editing, Supervision. **Wei Ren:** Resources, Conceptualization, Writing – review & editing, Supervision, Data curation. **Xubiao Luo:** Conceptualization, Writing – review & editing, Supervision.

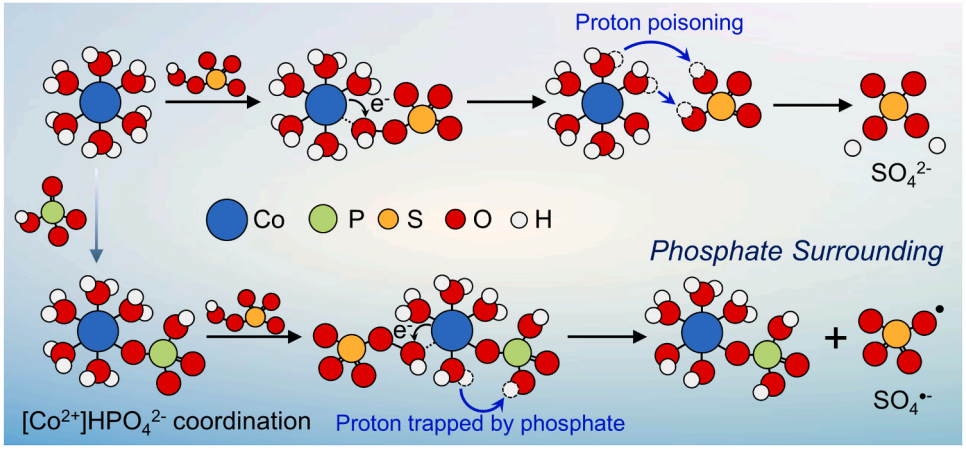

Fig. 6. Mechanism of the enhanced PMS activation by Co(II)-phosphate complex.

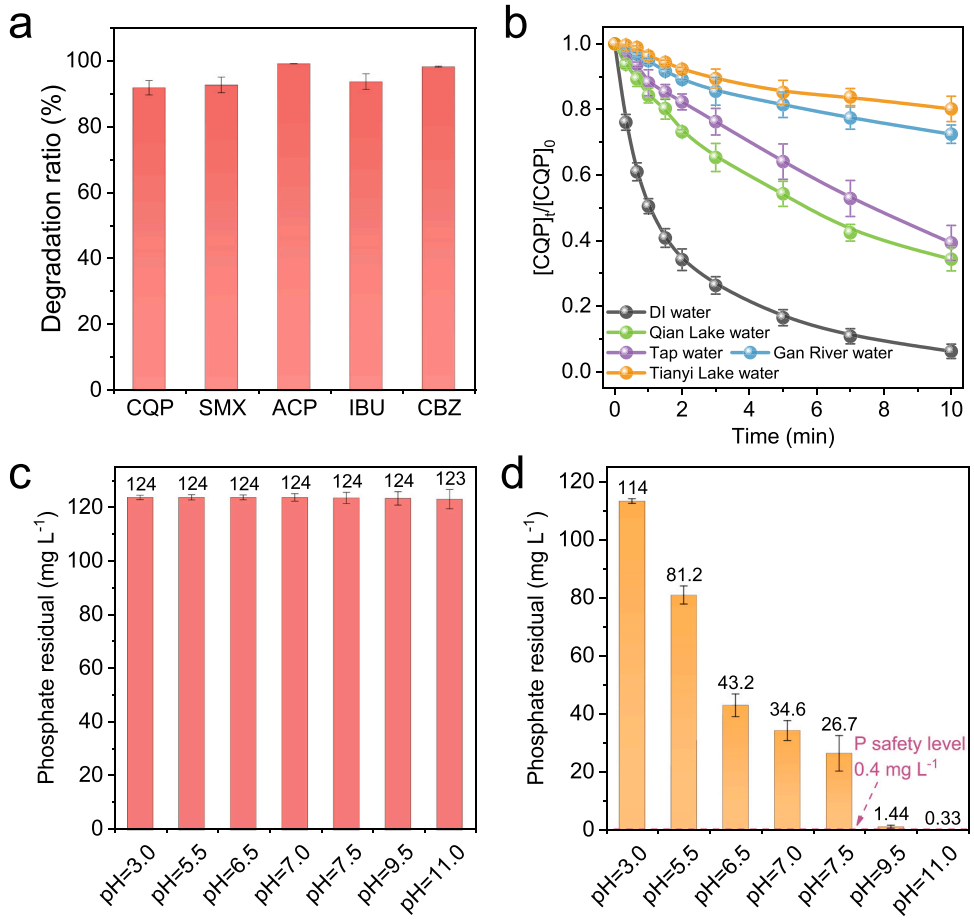

Fig. 7. (a) Degradation ratio of various pollutants in Co(II)+phosphate/PMS system. (b) Degradation performance of CQP in different real water. Phosphate residual by the treatment using (c) sole $CaCl_2$ and (d) $CaCl_2$ and polyferric sulfate combined methods at different pH values. Conditions: [Pollutant] = 6.0 μM, [Co(II)] = 0.8 μM, [phosphate] = 4.0 mM, [PMS] = 0.4 mM, pH 6.5 (in a and b).

Declaration of Competing Interest

The authors declare that they have no known competing financial interests or personal relationships that could have appeared to influence the work reported in this paper.

Data Availability

Data will be made available on request.

Acknowledgements

This study was financially supported by the National Natural Science Foundation of China (No. 52100090 and No. 52100147), the Provincial Natural Science Foundation of Jiangxi (No. 20224BAB213056, No. 20232BAB203035, No. 20224BAB213057 and No. 20232BAB204094), the National Science Fund for Distinguished Young Scholars (No. 52125002). C.C. gratefully acknowledges the China Scholarship Council for a one-year research grant (202106270136) at The University of Adelaide. This study was supported by the supercomputing service of Nanchang Hangkong University." should be added before this sentence..

Appendix A. Supporting information

Supplementary data associated with this article can be found in the online version at doi:10.1016/j.apcatb.2023.123616.

References

[1] J.L. Wang, L.J. Xu, Advanced oxidation processes for wastewater treatment: formation of hydroxyl radical and application, Crit. Rev. Environ. Sci. Technol. 42 (2012) 251–325.
[2] J. Lee, U. von Gunten, J.H. Kim, Persulfate-based advanced oxidation: critical assessment of opportunities and roadblocks, Environ. Sci. Technol. 54 (2020) 3064–3081.
[3] G.P. Anipsitakis, D.D. Dionysiou, Degradation of organic contaminants in water with sulfate radicals generated by the conjunction of peroxymonosulfate with cobalt, Environ. Sci. Technol. 37 (2003) 4790–4797.
[4] Y.H. Huang, Y.F. Huang, C.I. Huang, C.Y. Chen, Efficient decolorization of azo dye reactive black B involving aromatic fragment degradation in buffered Co^{2+}/PMS oxidative processes with a ppb level dosage of Co^{2+}-catalyst, J. Hazard. Mater. 170 (2009) 1110–1118.
[5] Y. Feng, G.G. Ying, Z. Yang, K. Shih, H. Li, D. Wu, Sulfate radical-induced destruction of emerging contaminants using traces of cobalt ions as catalysts, Chemosphere 256 (2020), 127061.
[6] H. Li, Z. Zhao, J. Qian, B. Pan, Are free radicals the primary reactive species in Co (II)-mediated activation of peroxymonosulfate? New evidence for the role of the Co (II)-peroxymonosulfate complex, Environ. Sci. Technol. 55 (2021) 6397–6406.
[7] B. Liu, W. Guo, H. Wang, S. Zheng, Q. Si, Q. Zhao, H. Luo, N. Ren, Peroxymonosulfate activation by cobalt(II) for degradation of organic contaminants via high-valent cobalt-oxo and radical species, J. Hazard. Mater. 416 (2021), 125679.
[8] M. Chen, L. Zhu, S. Liu, R. Li, N. Wang, H. Tang, Efficient degradation of organic pollutants by low-level Co^{2+} catalyzed homogeneous activation of peroxymonosulfate, J. Hazard. Mater. 371 (2019) 456–462.
[9] B. Huang, Z. Xiong, P. Zhou, H. Zhang, Z. Pan, G. Yao, B. Lai, Ultrafast degradation of contaminants in a trace cobalt(II) activated peroxymonosulfate process triggered through borate: indispensable role of intermediate complex, J. Hazard. Mater. 424 (2022), 127641.
[10] T. Li, Z. Zhao, Q. Wang, P. Xie, J. Ma, Strongly enhanced Fenton degradation of organic pollutants by cysteine: an aliphatic amino acid accelerator outweighs hydroquinone analogues, Water Res 105 (2016) 479–486.

[11] Y. Wang, Y. Wu, Y. Yu, T. Pan, D. Li, D. Lambropoulou, X. Yang, Natural polyphenols enhanced the Cu(II)/peroxymonosulfate (PMS) oxidation: the contribution of Cu(III) and $HO^{\bullet}$, Water Res 186 (2020), 116326.
[12] P. Zhou, Y. Yang, W. Ren, X. Li, Y. Zhang, B. Lai, S. Wang, X. Duan, Molecular and kinetic insights to boron boosted Fenton-like activation of peroxymonosulfate for water decontamination, Appl. Catal. B 319 (2022), 121916.
[13] S. Nam, V. Renganathan, P.G. Tratnyek, Substituent effects on azo dye oxidation by the FeIII–EDTA–H_2O_2 system, Chemosphere 45 (2001) 59–65.
[14] W. Huang, M. Brigante, F. Wu, C. Mousty, K. Hanna, G. Mailhot, Assessment of the Fe(III)–EDDS complex in Fenton-like processes: From the radical formation to the degradation of bisphenol A, Environ. Sci. Technol. 47 (2013) 1952–1959.
[15] J. Zhu, H. Li, C. Shan, S. Wang, L. Lv, B. Pan, Trace Co^{2+} coupled with phosphate triggers efficient peroxymonosulfate activation for organic degradation, J. Hazard. Mater. 409 (2021), 124920.
[16] J. Zhang, C. Shan, W. Zhang, B. Pan, In situ ligand-modulated activation of inert Ce (III/IV) into ozonation catalyst for efficient water treatment, Proc. Natl. Acad. Sci. USA 120 (2023), e2305255120.
[17] N. Li, Y. Wang, X. Cheng, H. Dai, B. Yan, G. Chen, L. Hou, S. Wang, Influences and mechanisms of phosphate ions onto persulfate activation and organic degradation in water treatment: a review, Water Res 222 (2022), 118896.
[18] C. Cheng, W. Ren, F. Miao, X. Chen, X. Chen, H. Zhang, Generation of Fe^{IV}=O and its contribution to Fenton-like reactions on a single-atom iron-N-C catalyst, Angew. Chem. Int. Ed. 62 (2023), e202218510.
[19] B. Wang, C. Cheng, M. Jin, J. He, H. Zhang, W. Ren, J. Li, D. Wang, Y. Li, A site distance effect induced by reactant molecule matchup in single-atom catalysts for Fenton-like reactions, Angew. Chem. Int. Ed. 61 (2022), e202207268.
[20] P. Duan, X. Liu, B. Liu, M. Akram, Y. Li, J. Pan, Q. Yue, B. Gao, X. Xu, Effect of phosphate on peroxymonosulfate activation: accelerating generation of sulfate radical and underlying mechanism, Appl. Catal. B 298 (2021), 120532.
[21] J. Ren, Y. Huang, J. Yao, S. Zheng, Y. Zhao, Y. Hou, B. Yang, L. Lei, Z. Li, D. D. Dionysiou, The role of reactive phosphate species in the abatement of micropollutants by activated peroxymonosulfate in the treatment of phosphate-rich wastewater, Water Res 243 (2023), 120341.
[22] P. Duan, Y. Qi, S. Feng, X. Peng, W. Wang, Y. Yue, Y. Shang, Y. Li, B. Gao, X. Xu, Enhanced degradation of clothianidin in peroxymonosulfate/catalyst system via core-shell FeMn @ N-C and phosphate surrounding, Appl. Catal. B 267 (2020), 118717.
[23] Y. Wen, V.K. Sharma, X. Ma, Activation of peroxymonosulfate by phosphate and carbonate for the abatement of atrazine: roles of radical and nonradical species, ACS EST Water 2 (2022) 635–643.
[24] J. Zhu, S. Wang, H. Li, J. Qian, L. Lv, B. Pan, Degradation of phosphonates in Co (II)/peroxymonosulfate process: performance and mechanism, Water Res 202 (2021), 117397.
[25] J. Wang, S. Wang, Effect of inorganic anions on the performance of advanced oxidation processes for degradation of organic contaminants, Chem. Eng. J. 411 (2021), 128392.
[26] Y. Zhang, M. Zhou, A critical review of the application of chelating agents to enable Fenton and Fenton-like reactions at high pH values, J. Hazard. Mater. 362 (2019) 436–450.
[27] F.P. Dwyer, D.P. Mellor, Chelating Agents and Metal Chelates, Elsevier, New York, 1964.
[28] H. Zhou, H. Zhang, Y. He, B. Huang, C. Zhou, G. Yao, B. Lai, Critical review of reductant-enhanced peroxide activation processes: trade-off between accelerated Fe^{3+}/Fe^{2+} cycle and quenching reactions, Appl. Catal. B 286 (2021), 119900.
[29] B. Wu, J. Wan, Y. Zhang, B. Pan, I.M.C. Lo, Selective phosphate removal from water and wastewater using sorption: process fundamentals and removal mechanisms, Environ. Sci. Technol. 54 (2020) 50–66.
[30] W. Stumm, J.J. Morgan. Aquatic Chemistry-chemical Equilibria and Rates in Natural Waters, Third ed.,, John Wiley & Sons, New York, 1996.
[31] Y. Zong, X. Guan, J. Xu, Y. Feng, Y. Mao, L. Xu, H. Chu, D. Wu, Unraveling the overlooked involvement of high-valent cobalt-oxo species generated from the cobalt(II)-activated peroxymonosulfate process, Environ. Sci. Technol. 54 (2020) 16231–16239.
[32] J. Song, N. Hou, X. Liu, M. Antonietti, P. Zhang, R. Ding, L. Song, Y. Wang, Y. Mu, Asymmetrically coordinated CoB_1N_3 moieties for selective generation of high-valence Co-oxo species via coupled electron-proton transfer in Fenton-like reactions, Adv. Mater. 35 (2023), e2209552.
[33] R.G. Parr, W. Yang, Density functional approach to the frontier-electron theory of chemical reactivity, J. Am. Chem. Soc. 106 (1984) 4049–4050.
[34] G. Kresse, J. Furthmüller, Efficiency of ab-initio total energy calculations for metals and semiconductors using a plane-wave basis set, Comput. Mater. Sci. (1) (1996) 15–50.
[35] X. Lou, L. Wu, Y. Guo, C. Chen, Z. Wang, D. Xiao, C. Fang, J. Liu, J. Zhao, S. Lu, Peroxymonosulfate activation by phosphate anion for organics degradation in water, Chemosphere 117 (2014) 582–585.
[36] C. Cheng, S. Gao, J. Zhu, G. Wang, L. Wang, X. Xia, Enhanced performance of $LaFeO_3$ perovskite for peroxymonosulfate activation through strontium doping towards 2,4-D degradation, Chem. Eng. J. 384 (2020), 123377.
[37] J.H. Wu, F. Chen, T.H. Yang, H.Q. Yu, Unveiling singlet oxygen spin trapping in catalytic oxidation processes using in situ kinetic EPR analysis, Proc. Natl. Acad. Sci. USA 120 (2023), e2305706120.
[38] Z. Wang, J. Wang, B. Xiong, F. Bai, S. Wang, Y. Wan, L. Zhang, P. Xie, M. R. Wiesner, Application of cobalt/peracetic acid to degrade sulfamethoxazole at neutral condition: Efficiency and mechanisms, Environ. Sci. Technol. 54 (2020) 464–475.
[39] G.V. Buxton, C.L. Greenstock, H.W. Phillip, A.B. Ross, Critical review of rate constants for reactions of hydrated eletrons, hydrogen atoms and hydroxyl radicals ($^{\bullet}OH$/$^{\bullet}O^-$) in aqueous solution, J. Phys. Chem. Ref. Data 17 (1988) 513–886.
[40] Q.Y. Wu, Z.W. Yang, Z.W. Wang, W.L. Wang, Oxygen doping of cobalt-single-atom coordination enhances peroxymonosulfate activation and high-valent cobalt-oxo species formation, Proc. Natl. Acad. Sci. USA 120 (2023), e2219923120.
[41] P. Neta, R.E. Huie, A.B. Ross, Rate constants for reactions of inorganic radicals in aqueous solution, J. Phys. Chem. Ref. Data 17 (1988) 1027–1284.
[42] X.-H. Yi, H. Ji, C.-C. Wang, Y. Li, Y.-H. Li, C. Zhao, A. Wang, H. Fu, P. Wang, X. Zhao, W. Liu, Photocatalysis-activated SR-AOP over PDINH/MIL-88A(Fe) composites for boosted chloroquine phosphate degradation: performance, mechanism, pathway and DFT calculations, Appl. Catal. B 293 (2021), 120229.
[43] W. Ren, Q. Zhang, C. Cheng, F. Miao, H. Zhang, X. Luo, S. Wang, X. Duan, Electro-induced carbon nanotube discrete electrodes for sustainable persulfate activation, Environ. Sci. Technol. 56 (2022) 14019–14029.
[44] Y. Peng, Q. Zhang, W. Ren, X. Duan, L. Ding, Y. Jing, P. Shao, X. Xiao, X. Luo, Thermodynamic and kinetic behaviors of persulfate-based electron-transfer regime in carbocatalysis, Environ. Sci. Technol. 57 (2023) 19012–19022.
[45] L. Chen, H. Ji, J. Qi, T. Huang, C.-C. Wang, W. Liu, Degradation of acetaminophen by activated peroxymonosulfate using $Co(OH)_2$ hollow microsphere supported titanate nanotubes: Insights into sulfate radical production pathway through $CoOH^+$ activation, Chem. Eng. J. 406 (2021), 126877.
[46] C. Ehrhardt, M. Gjikaj, W. Brockner, Thermal decomposition of cobalt nitrato compounds: preparation of anhydrous cobalt(II)nitrate and its characterisation by Infrared and Raman spectra, Thermochim. Acta 432 (2005) 36–40.
[47] G. Niaura, A.K. Gaigalas, V.V. L, Surface-enhanced raman spectroscopy of phosphate anions: adsorption on silver, gold, and copper electrodes, , J. Phys. Chem. B 101 (1997) 9250–9262.
[48] T. Zhang, H. Zhu, J.P. Croue, Production of sulfate radical from peroxymonosulfate induced by a magnetically separable $CuFe_2O_4$ spinel in water: Efficiency, stability, and mechanism, Environ. Sci. Technol. 47 (2013) 2784–2791.
[49] A.J. Bard, L.R. Faulkner. Electrochemical Methods: Fundamentals and Applications, Second ed.,, John Wiley & Sons, Inc, Hoboken, New Jersey, 2001.
[50] J. Luo, N.P. Rath, L.M. Mirica, Dinuclear Co(II)Co(III) mixed-valence and Co(III)Co (III) complexes with N- and O-donor ligands: characterization and water oxidation studies, Inorg. Chem. 50 (2011) 6152–6157.
[51] C. Chu, J. Yang, X. Zhou, D. Huang, H. Qi, S. Weon, J. Li, M. Elimelech, A. Wang, J. H. Kim, Cobalt single atoms on tetrapyridomacrocyclic support for efficient peroxymonosulfate activation, Environ. Sci. Technol. 55 (2021) 1242–1250.
[52] J. Cui, X. Wang, J. Zhang, X. Qiu, D. Wang, Y. Zhao, B. Xi, A.N. Alshawabkeh, X. Mao, Disilicate-assisted iron electrolysis for sequential Fenton-oxidation and coagulation of aqueous contaminants, Environ. Sci. Technol. 51 (2017) 8077–8084.
[53] L. Lian, B. Yao, S. Hou, J. Fang, S. Yan, W. Song, Kinetic study of hydroxyl and sulfate radical-mediated oxidation of pharmaceuticals in wastewater effluents, Environ. Sci. Technol. 51 (2017) 2954–2962.